

# Caged clusters in $\text{Al}_{11}\text{Ir}_4$ : structural transition and insulating phase

Marek Mihalkovič<sup>1</sup> and C. L. Henley<sup>2</sup>

<sup>1</sup> *Institute of Physics, Slovak Academy of Sciences, 84511 Bratislava, Slovakia.*

<sup>2</sup> *Laboratory of Atomic and Solid State Physics, Cornell University, Ithaca, NY, 14853-2501*

Using pair potentials fitted to an ab-initio database, combined with replica-exchange simulated annealing, we show the complex, quasicrystal-related  $\text{Al}_{11}\text{Ir}_4$  compound contains a new version of the “pseudo-Mackay” icosahedral cluster, with non-icosahedral inner  $\text{Al}_{10}\text{Ir}$  and/or  $\text{Al}_9\text{Ir}$  clusters that exist in various orientations and account for partial occupancies in the reported structure. Two different compositions show first-order transitions to orientationally ordered phases doubling the (cubic) unit cell, which are respectively metallic and insulating.

PACS numbers: 02.70.Ns, 61.50.Lt, 63.20.Dj, 64.70.Kb, 61.44.Br

$\text{Al}_{11}\text{Ir}_4$  is a phase in one of the complex metallic alloy systems that resist ordinary approaches to determining crystallographic structure or phase diagrams, because of two impediments to equilibration at low temperatures: (1) there are numerous competing complex phases of similar composition (2) the intermediate-temperature structures have inherent entropy associated with *block rearrangements* of tiles or clusters.

Despite the measurement of 457 independent reflections, the experimentally refined structure [1] of  $\text{Al}_{11}\text{Ir}_4$  has twice as many sites listed as atoms, many with a fitted occupancy of less than 0.5. Until occupancy correlations are known, such structure knowledge is inadequate for computing electronic properties or total energies.

Instead, in this letter we *predict* the structure, aided by its close relationship to Al-transition metal (Al-TM) quasicrystals. These are described as networks of identically oriented icosahedral clusters linked along certain symmetry directions [2], e.g. the “Mackay icosahedron” [2] consisting of an empty center plus two concentric shells of full icosahedral symmetry,  $\text{Al}_{12} + \text{Al}_{30}\text{Mn}_{12}$ . It is generally accepted that the stable quasicrystals *i*-AlCuFe and *i*-AlPdMn contain a modified cluster called the “pseudo Mackay icosahedron” (pMI) in which the inner  $\text{Al}_{12}$  icosahedron is replaced by a cluster with fewer atoms and reduced symmetry [3], the details of which are still unclear. We note that the Ca–Cd quasicrystals, another major class alongside the Al–TM quasicrystals, and complex alloys related to them, also contain icosahedral clusters with an inner shell of lower symmetry [4] – a tetrahedron, in that case. Thus, such inner rotatable clusters may be a common feature of well-ordered quasicrystal systems, and they present tractable examples of the above-mentioned block-rearrangement degrees of freedom.

In the rest of this paper, we uncover the correct low- $T$  structure of  $\text{Al}_{11}\text{Ir}_4$  using energy minimization, in several stages. We used both ab-initio codes (VASP package [5]) and empirically fitted pair potentials. First we determined the possible atom contents of one cluster to be  $\text{Al}_9\text{Ir}$  or  $\text{Al}_{10}\text{Ir}$ . Next, for each cluster, we find its atom arrangement and preferred orientation within the cage of

neighboring atoms. The partially occupied sites in the refined structure [1] are explained with an equal mixture of the two kinds of cluster. We also find the collective ordering of orientations and identify the ordering transition. The equal-mixture phase is metallic, as seen in experiment [25], but the composition with  $\text{Al}_{10}\text{Ir}$  clusters is predicted to be insulating.

As a prerequisite to exploring alternative structures and running extensive molecular dynamics (MD) simulations, we generated “empirical oscillating pair potentials” (EOPP) valid for Al–Ir in this composition range, using the method of Ref. [6] to fit a database of ab-initio forces, calculated with VASP [5]. The database contained snapshots from ab-initio molecular dynamics simulations at high temperatures, as well as  $T = 0$  structures of various stable and unstable Al–Ir structures, in particular the  $\text{Al}_{21}\text{Pd}_8$  and  $B2$  structures. (The functional form and fitted coefficients of the potentials are provided in the supplementary material [10].)

*Structural optimization of individual cluster in  $\text{Al}_{11}\text{Ir}_4$*  — The reported crystal structure of  $\text{Al}_{11}\text{Ir}_4$  is a simple cubic arrangement of pMI clusters, each having an inner shell of  $\sim 40$  partially occupied sites with combined occupancy 10. Surrounding this is the second shell, an  $\text{Ir}_{12}$  icosahedron, plus 30 Al sites slightly outside that icosahedron’s mid-edges, of which the six sites along cubic 2-fold axes are only partially occupied. Between the pMI clusters, at each body center, is an Ir atom, surrounded by an icosahedron of 12 Al atoms, which are shared with the pMI in the role of second-shell Al. The key fact to determine by energy optimization is the atom configuration in the uncertain, inner-shell sites.

The first question about the inner Al cluster is how many atoms it (optimally) contains. We addressed this directly by constructing initial configurations of the  $\text{Al}_{11}\text{Ir}_4$  unit cell with a chosen number  $m$  of inner Al atoms (assuming the periodicity of only one unit cell). The configuration was optimized, first by annealing with molecular dynamics (MD) using the fitted EOPP potentials at fixed volume; this was followed by ab-initio relaxation using VASP [5], optimizing all structural parameters. [9]. The first stage was annealing in one unit cell

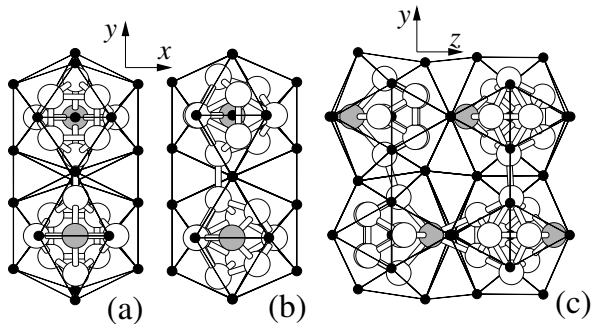


FIG. 1: Inner clusters in  $\text{Al}_{11}\text{Ir}_4$  structures, shown as they order in the low- $T$  “9.5 phase”. The surrounding icosahedron of black atoms is the  $\text{Ir}_{12}$  “cage”; another Ir atom is at center. The “apex” Al atoms are shown gray. (a).  $\text{Al}_9\text{Ir}$  clusters in  $z = 0$  plane of the “9.5 phase” with their 4-fold axes oriented up and down along viewing  $z$  axis, (b).  $\text{Al}_{10}\text{Ir}$  clusters in  $z = 0.5$  plane, with their 3-fold axis almost parallel to the viewing  $z$  axis. (c). Orientation relation of two  $\text{Al}_9\text{Ir}$  clusters (left) with two  $\text{Al}_{10}\text{Ir}$  clusters (right), viewed along  $x$  direction. The layers of identical-content clusters are stacked normal to the page in (a) and (b), or left to right in (c), in a checkerboard pattern. In the 10 phase, 10-cluster arrangement in (b) is repeated in  $2 \times 1 \times 1$  supercell.

inner cluster Al	8	9	9.5	10	11	12
$1 \times 1 \times 1$	+45	+33	–	+10	+77	+132
supercell	–	+18	+9	+4	–	–
$a_{\text{cub}} [\text{\AA}]$	7.64	7.68	7.70	7.73	7.78	7.82

TABLE I: Relaxed energies (in meV/atom) as a function of Al per pMI inner cluster. Supercell used was  $2 \times 2 \times 2$ , except  $4 \times 4 \times 4$  for the 10 Al case. Last row is mean lattice parameter, per fundamental cell.

(see Table I), to identify gross energy differences: this excluded the  $m = 8$ ,  $m = 11$  and  $m = 12$  variants, leaving only the  $m = 9$  and  $m = 10$  ones which we “9-cluster” and “10-cluster” from here on. In a second stage, we annealed in a supercell to accommodate possible alternations of the orientations, and found two nearly stable structures: the  $m = 10$  filling (“10-phase”) and an equal mixture of  $m = 9$  and  $m = 10$  fillings (“9.5-phase”). From here on, in studies of the whole structure, we limit ourselves to these two fillings.

The 9-cluster is almost always a square antiprism, with one square enlarged and capped by an additional Al atom [see Fig.1(a)]. In its optimum orientation (of multiplicity six), the fourfold axis is aligned with one of the cubic  $\langle 100 \rangle$  axes, with the outer square of atoms in mirror planes. The 10-cluster is practically always a sort of trigonal prism, with one triangular end face enlarged and capped by an atom, and also capped on the three trapezoidal side faces.

In its optimum orientation (of multiplicity 12), the 10-cluster is tilted rigidly so as to bring its threefold axis closer to (but not quite parallel to) the nearby  $\langle 100 \rangle$  axis, as seen in Figure 1(b). That brings the apical capping Al and all three of the side-capping Al atoms (which are farther out from the central Ir) close to cubic  $\langle 100 \rangle$  axes, and they merge with the Al atoms of the pMI’s second shell (cage) that sit in the same direction. The pMI clusters in Fig. 1 *overlap* along the  $[100]$  direction such that some outer shell atoms of one pMI also belong to the inner cluster of the neighboring pMI [12].

At  $T \cong 600\text{K}$ , just 100K above the orientational  $T_c$  (see below), an inner  $\text{Al}_{10}\text{Ir}$  cluster spends 95% of the time close to one of the twelve ideal orientations described above (as shown by quenching a crystal using  $\text{Al}_{10}$  filling in each cage.) At higher temperatures, the threefold axis of the 10-cluster may instead align along a cubic  $\langle 111 \rangle$  axis, or a pseudo 2-fold axis (of the  $\text{Ir}_{12}$  cage). (We have not examined the high- $T$  orientations of the 9-cluster.)

The Al partial occupancies refined in [1] are in close agreement with our model, provided that close to half the clusters are 9-clusters and half are 10-clusters, and each is oriented independently in one of the (respectively) six or 12 optimum orientations. [11] (Fig. 2(a) shows the time-averaged atom density from a high- $T$  simulation, containing lines of closely spaced alternative sites. The refined Al(3) and Al(4) sites of [1] represent this spread-out density, coming from four or five model sites of both 9- and 10-clusters; the reported Al(2) and Al(5) sites comes respectively from one site of the 9-cluster and two sites of the 10-cluster in our model, showing that both clusters must be present. The r.m.s. discrepancy between predicted and reported occupancies of each site is  $\sim 12\%$  of the occupancy [10].

*Orientational ordering* — To address the statistical mechanics of systems with many interacting clusters, we set up a replica-exchange [7] simulation in a  $4 \times 4 \times 4$  supercell, i.e. 1920 atoms (10-phase), annealing 16 independent samples, each at a different temperature, spanning 310K to 460K; additional single- $T$  simulations were done at higher temperatures.

The simulated alloy remains solid beyond 1700 K in  $2 \times 2 \times 2$  supercell (the experimental melting point is above 1600 C for  $x_{\text{Ir}} \sim 0.27$  [13]). The simulation lasted 4000 cycles, each consisting of 1000 molecular dynamics (MD) steps with time increment  $\Delta t = 5$  fs, for a total simulation time 20 ns. The pair-potential interaction radius was cut off at  $r_c = 10 \text{\AA}$ . [8]. The initial state for the MD was our best single-cell model, repeated in all  $4^3$  cells.

The *low-temperature* optimal structures of the 9.5-phase and 10-phase were determined by rapidly quenching configurations from the lowest replica ( $T = 310\text{K}$ ) to a  $T = 0$  energy minimum, and selecting those with the lowest relaxed energies. In 9.5-phase, the structure was a stack along (say) the  $z$  direction of layers which

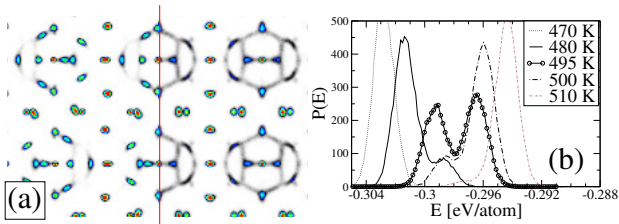


FIG. 2: Disordered and ordered states of inner clusters. Phase transition in the “10” phase from replica-exchange molecular dynamics simulation in  $4 \times 4 \times 4$  supercell of the basic (30-atom) unit cell. simulation results from  $4 \times 4 \times 4$  supercell of the basic (30-atom) unit cell. (a) time-averaged occupancy distributions for a slice of thickness  $6 \text{ \AA}$  taken through the  $4 \times 4 \times 4$  supercell of the “10” phase composition, below the ordering transition at  $T = 470 \text{ K}$  (left) and above it at  $510 \text{ K}$  (right). (b) Probability distribution  $P(E)$  for total energy (normalized per atom) of the “10” composition, at five temperatures from  $470 \text{ K}$  to  $510 \text{ K}$ ; the double peak at  $480 \text{ K} \leq T \leq 500 \text{ K}$  is diagnostic of coexistence and a first-order phase transition.

structure	Pearson symbol	Space group	parameters ( $\text{\AA}$ )			Al	Ir
			$a$	$b$	$c$		
Ref. 1	cP60	$P23$	7.67	(cubic)		22	8
high- $T$ 9.5	cP178	$Pm\bar{3}$	7.73	(cubic)		21.5	8
9.5-phase	oA236	$Abm2$	15.48	15.41	15.32	172	64
10-phase	oP60	$Pma2$	15.49	7.74	7.70	44	16

TABLE II: Crystal data for  $\text{Al}_{11}\text{Ir}_4$  structures, from diffraction refinement [1], the disordered high- $T$  9.5-state and the ordered states of the 9.5-phase and 10-phase. Columns include lattice constants and Al or Ir atoms per cell. For “high- $T$ ” 9.5, data in “(…)” are from Ref. 1.

had a  $\sqrt{2} \times \sqrt{2}$  checkerboard pattern of inner clusters, with their main (fourfold or threefold) axes alternating between  $+z$  and  $-z$  directions; the layers are stacked such that the overlaying clusters have the same orientation of main axes. (To fully specify their orientations, note the 10-clusters of  $+z$  and  $-z$  alignment are always related by a mirror reflection in the  $xy$  plane.) The relation between adjoining clusters is shown in Figure 1. In the 10-phase, the 10-clusters pair shown in Fig. 1(b) is repeated in the supercell doubled along  $y$  direction. The crystal structures are summarized in Table II; coordinates are available in Ref. [10].

The ordered arrangement of the 9.5 phase contains alternating (square) layers of 9-clusters and 10-clusters. Each layer is made by repeating Fig. 1(a) or (b) in both directions: thus, within either kind of layer, the apex directions alternate up and down. These layers are stacked without shifts so that chains of identically aligned clusters run perpendicular to the plane of the layers.

We pinpointed the ordering temperature of the “10” phase in three ways. Firstly, we can examine the atom density distribution, averaged over moderate times (Fig. 2(a); for  $T > T_c$  this has the full symmetry of the unit cell, but for  $T < T_c$  this shows (despite some fluctuations) a clear symmetry breaking (to the cell-doubled structure just described). A second evidence for a phase transition is available within the replica-exchange simulation: a larger energy spacing  $\Delta \bar{E}_i = E(T_i) - E(T_{i-1})$  between the replicas at consecutive temperatures, suggesting a latent heat. The third and most convincing signature is that, for a finite system, the ensemble at temperatures close to  $T_c$  is a mixture of the two phases, weighted according to the difference in their free energies. This is evident in Fig. 2(b), from which we can read off  $T_c \lesssim 495 \text{ K}$ . The peak separation in Fig. 2(b) shows that the ordered and disordered states in the 10-phase differ by (a latent heat of)  $3 \text{ meV}$  per atom, requiring an entropy difference at  $T_c$  of  $(30)(3 \text{ meV})/T_c \approx \ln(9)$  per 30-atom cell. That is, we have effectively  $N_{cs} \approx 9$  states per cluster, comparable with  $N_{cs} = 12$  ideal orientations.

The 9.5 phase has two kinds of order – the 9Al/10Al alternation in cluster content and the orientations – which might appear in separate transitions. The first ordering requires vastly longer equilibration times (for inter-cluster Al diffusion) and we were unable to identify any sharp transitions.

*Phase stability in Al-Ir system* — We now turn to the  $T = 0$  phase stability of  $\text{Al}_{11}\text{Ir}_4$  and other Al-Ir compounds. The currently accepted Al-Ir phase diagram [13] with  $0 < x_{\text{Ir}} \leq 0.5$  shows six compounds as stable:  $\text{Al}_9\text{Ir}_2$  (in the  $\text{Al}_9\text{Co}_2$  mP22 structure); AlIr; and around  $x_{\text{Ir}} \approx 1/4$ , there is  $\text{Al}_3\text{Ir}$  plus the complex phases  $\text{Al}_{11}\text{Ir}_4$ ,  $\text{Al}_{28}\text{Ir}_9$  [14] and orthorhombic  $\text{Al}_{45}\text{Ir}_{13}$  [15]. We additionally tried other complex phases structures not reported in Al-Ir, among them: (i)  $\text{Al}_{21}\text{Ir}_8$  in the  $\text{Al}_{21}\text{Pd}_8$  structure, [16] which is a packing of sixteen of our 10-clusters per unit cell, *without* any icosahedral cages (and sharing a few Al atoms). (ii)  $\text{Al}_{41}\text{Ir}_{23}$  in the  $\text{Al}_{41}\text{Cu}_8\text{Ir}_{15}$  structure [18], equivalent to  $\text{Al}_{68}\text{Pd}_{20}\text{Ru}_{12}$  [19] and Al-CuRuSi [20]; here the even-vertex clusters alternate between an  $\text{Al}_{10}\text{Ir}$  trigonal cluster and an  $\text{AlCu}_8\text{Al}_6$  cluster, identical to atomic arrangement in  $B2$  cubic structure.

Of these, the available structures of  $\text{Al}_{11}\text{Ir}_4$  and  $\text{Al}_{28}\text{Ir}_9$  include many fractional sites, so in total energy calculations we had to try versions of these structures with various ways of realizing the occupations. The relaxed total energies of all these compounds (and the pure elements) were computed using VASP [5]. We found AlIr and  $\text{Al}_9\text{Ir}_2$  to be stable, as expected; the only stable phases around  $x_{\text{Ir}} \approx 1/4$  were  $\text{Al}_{45}\text{Ir}_{13}$  and (surprisingly)  $\text{Al}_{21}\text{Ir}_8$ . Relative to a corrected tie-line including  $\text{Al}_{21}\text{Ir}_8$ , we found  $\text{Al}_3\text{Ir}$  to be unstable by  $25 \text{ meV/atom}$ ; this is reduced to only  $\sim 8 \text{ meV/atom}$  in a variant ( $\text{Al}_{17}\text{Ir}_6$ ) with a tripled cell in which one Al is removed. Thus, in contradiction to Ref. 13, we believe  $\text{Al}_3\text{Ir}$  is a high-temperature

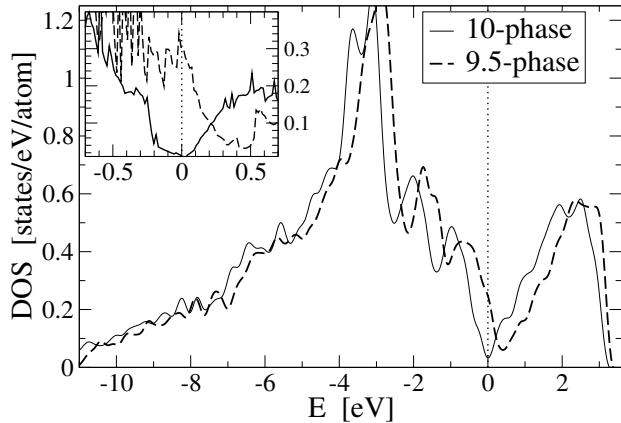


FIG. 3: Electronic density of states (DOS) of  $T = 0$  ordered structures, where  $E = 0$  is the Fermi energy; (curves are smoothed using the Methfessel-Paxton smearing method). The 10-phase has a gap of  $\sim 40$  meV (blown up in inset, tetrahedron method) but in the 9.5 phase, the Fermi level is  $\sim 0.5$  eV shifted from a pseudogap.

phase only. The phases  $\text{Al}_{41}\text{Ir}_{23}$ ,  $\text{Al}_{28}\text{Ir}_9$ , and  $\text{Al}_{11}\text{Ir}_4$  in the 9.5-phase were unstable by rather small amounts of 6, 7, and 9 meV/atom, respectively; in the latter two, the site disorder contributes entropy which may explain their stability at higher temperatures. The heat of formation for  $\text{Al}_{11}\text{Ir}_4$  is large:  $-0.738$  eV/atom; for  $\text{Al}_{21}\text{Ir}_8$  it is  $-0.760$  eV/atom (see Supplementary material for detailed information on formation energies and stability data for all discussed phases).

*Electronic density of states* — A specific interest in Al-Ir and certain other Al-TM systems is the possibility of an insulating alloy, the elemental constituents of which are all good metals, e.g.  $\text{Al}_2\text{Ru}$  in the  $\text{TiSi}_2$  structure [21]  $\text{Al}_2\text{Fe}$  in the  $\text{MoSi}_2$  type-structure [21, 22]. Quasicrystal  $i\text{-AlPdRe}$  (built from pMI clusters) is long claimed to be a semiconductor [23, 24]. Predicting gap formation in these alloys depends critically on the accurate relaxation of atomic positions [23].

We find the  $\text{Al}_{11}\text{Ir}_4$  electronic density of states (DOS) in the ordered ( $T = 0$ ) “10” phase has a narrow gap, and significant pseudogap as shown in Fig. 3, so this alloy should be a semiconductor. By contrast, the ordered “9.5” phase is predicted to be robustly metallic [Fig. 3(b)] (In the disordered high-temperature “10” phase [not shown] the gap tends to get filled in, so that phase is also likely to be metallic.) We call attention to the fact that these very similar structures have radically different electronic properties, all due to details of the placement of certain Al atoms that link adjacent clusters.

*Discussion* — In conclusion, starting from diffraction-data refined average structure of  $\text{Al}_{11}\text{Ir}_4$ [1], we com-

bined molecular dynamics simulations with pair potentials to discover a well-defined, asymmetric inner  $\text{Al}_9\text{Ir}$  and  $\text{Al}_{10}\text{Ir}$  clusters, with variable orientations, and an ordering transition to new orthorhombic phases. We suggest an experimental search for the ordered phase having all clusters of  $\text{Al}_{10}\text{Ir}$  type, as it has a *gap* exactly at the Fermi energy, and hence should be a semiconductor. We also found that, contrary to the accepted phase diagram, the stable low-temperature phase at  $x_{\text{Ir}} \approx 1/4$  is  $\text{Al}_{21}\text{Ir}_8$ .

Several other known structures are made by placing pMI clusters and/or variants on the same simple cubic lattice with  $a \sim 7.7\text{\AA}$ : not only  $\text{Al}_{41}\text{Cu}_8\text{Ir}_{15}$ , [18],  $\text{Al}_{68}\text{Pd}_{20}\text{Ru}_{12}$  [19] and  $\text{AlCuRuSi}$  [20], which we mentioned, but also  $\text{Al}_{70}\text{Pd}_{10}\text{Fe}_{20}$  [29], and  $\epsilon\text{-Ag}_7\text{Mg}_{26}$  (in the latter case, the “even”-node inner clusters are  $\text{AgMg}_8$  cube, while “odd” nodes are perfect Mackay icosahedra).

Furthermore, the lowest energy version yet found of the  $i\text{-AlPdMn}$  quasicrystal structure [26, 27] consists of exactly the same pMI clusters described above, in particular (i) they have a short ( $\sim 8\text{\AA}$ ) linkage along the icosahedral twofold direction, rather than the  $\sim 12.5\text{\AA}$  linkage known from  $\alpha\text{-AlMnSi}$  [2] (ii) they have an  $\text{Al}_{10}\text{Mn}$  inner cluster in the same shape as the one described here, which appear in various orientations with only small energy differences. The decagonal-related  $\xi'(\text{AlPdMn})$  phase contains pMI clusters with  $\text{Al}_9\text{Mn}$  and  $\text{Al}_{10}\text{Mn}$  inner clusters, not quite identical to those we presented here.

The icosahedral cage containing an inner cluster that breaks icosahedral symmetry is known in a quite different family of quasicrystals and related compounds:  $\text{CaCd}_6$  or  $\text{ScZn}_6$ , with an inner  $\text{Cd}_4$  or  $\text{Zn}_4$  tetrahedron [4, 30]. Those, too, show orientational orderings at low temperatures [31, 32]. We observe that, if there is any way at all in icosahedral quasicrystals to implement the long-sought “local matching rules” that would stabilize an ideal quasiperiodic ground state, or merely rules that limit tiling randomness to large spatial scales the likeliest candidate are these inner clusters that spoil the clusters’ high symmetry.

On the theoretical side, this work on Al-Ir could be extended in the following directions: (1) simulation of the inner-cluster dynamics for comparison to neutron data, analogous to the  $\text{Cd}_4$  tetrahedron in  $\text{CaCd}_6$  [30]; (2) fitting an orientational interaction between adjacent clusters [33] for Monte Carlo estimation of the orientational  $T_c$ . (3) a possible Al-Ir quasicrystal based on these clusters. Experimental clarification of the low-temperature stabilities of Al-Ir around  $x_{\text{Ir}} \sim 0.27$  are of course highly desirable.

We thank W. Steurer and P. Kuczera for sharing structural data on  $\text{Al}_{41}\text{Cu}_8\text{Ir}_{15}$  phase prior to publication, R. Tamura for fruitful discussions, and Yu. Grin for careful reading of the manuscript and comments, in particular pointing out cluster relationship with  $\text{Al}_6\text{Mn}$  structure. This work was supported by DOE Grant DE-FG02-

89ER-45405 (MM, CLH), and Slovak funding VEGA 2/0111/11 and APVV-0492-11 (MM).

- 
- [1] Y. Grin, K. Peters, U. Burkhardt, K. Gotzmann and M. Ellner : Z. Krist. **212**, 439 (1997)
- [2] V. Elser and C. L. Henley, Phys. Rev. Lett. 55, 2883 (1985).
- [3] A. Katz and D. Gratias, J. Non-Cryst. Solids **153-154** 187 (1993).
- [4] C. P. Gomez and S. Lidin, Phys. Rev. B 68, 024203 (2003).
- [5] (a) G. Kresse and J. Hafner, Phys. Rev. B, 47, R558 (1993); (b) G. Kresse and J. Furthmuller, Phys. Rev. B 54, 11169 (1996).
- [6] M. Mihalkovič and C. L. Henley, Phys. Rev. B **85**, 092102 (2012)
- [7] K. Hokushima and K. Nemoto, J. Phys. Soc. Jpn 65, 1604 (1996).
- [8] The portion of the potentials between 7–10Å is crucial for (even mechanical) stability.
- [9] Supercells are essential here, as adjacent clusters have different orientations in the low-energy states.
- [10] See supplementary information of this paper.
- [11] Of the two possible space groups suggested in Ref. [1], we must use  $Pm\bar{3}$ , which has inversion symmetry.
- [12] This is exactly the linkage of length  $\sim 7.8$  Å along a two-fold axis that was proposed by for the pMI network to describe *i*-AlPdMn, in V. Elser, Philos. Mag. B 73, 641 (1996). (We differ from Elser regarding the inner cluster details and the linkages along threefold axes.)
- [13] H. Okamoto, J. of Phase Equil. and Diffusion **30**, 206 (2009)
- [14] S. Katrych, V. Gramlich, and W. Steurer, J. Alloys Compd. 407, 132 (2006)
- [15] M. Boström, R. Niewa, Y. Prots, and Y. Grin, J. of Sol. State Chem. 178, 339 (2005)
- [16] K.-J. Range and E.G. Christl, J. Less-Common Met. 136 (1988) 277.
- [17] Y. Grin has pointed out that our 10-cluster is identical to the uncaged cluster from which Al<sub>6</sub>Mn is built [A. D. I. Nickol, Acta Crystallogr. 6, 285 (1953)].
- [18] P. Kuczera, W. Steurer, unpublished.
- [19] S. Mahne and W. Steurer Z. Kristallogr. 211, 17 (1996).
- [20] K. Sugiyama, T. Kato, K. Saito and K. Hiraga, Phil. Mag. Lett., 77, 165 (1998).
- [21] M. Weinert and R. E. Watson, Phys. Rev. 58, 9732 (1998); M. Krajčí and Hafner, J. Phys. Condens. Matter 14, 2002, p 5755; M. Krajčí and Hafner, J. Phys. Condens. Matter 14, 2002, p 7201
- [22] M. Mihalkovič and M. Widom, Phys. Rev. B. 85, 014113 (2012)
- [23] M. Krajčí and J. Hafner, Phys. Rev. B 75, 024116 (2007); M. Krajčí and Hafner, Phys. Rev. B 68, 165202 (2003).
- [24] F. S. Pierce, Q. Guo, and S. J. Poon, Phys. Rev. Lett. 73, 2220 (1994)
- [25] A. Oishi, K. Nishimoto, and R. Tamura, Z. Kristallogr. 224, 115 (2009).
- [26] M. Krajčí and J. Hafner, Phys. Rev. B 78, 224207 (2008)
- [27] M. Mihalkovič, C. L. Henley, and M. Krajčí, unpublished.
- [28] B. Frigan, A. Santana, M. Engel, D. Schopf, H.-R. Tre-

- bin, and M. Mihalkovič, Phys. Rev. B 84, 184203 (2011)
- [29] S. O. Balanetskii, B. Grushko, K. Urban, and T. Ya. Velikanova, Powder metallurgy and Metal Ceramics 43, 396 (2004).
- [30] M. Mihalkovič and C. L. Henley, Philos. Mag. 91, 2548 (2011).
- [31] T. Watanuki, A. Machida, T. Ikeda, K. Aoki, H. Kaneko, T. Shobu, T. J. Sato, and A. P. Tsai, Phys. Rev. Lett. 96, 105702 (2006).
- [32] T. Hatakeyama, K. Nozawa, and Y. Ishii, Z. Kristallogr. 223, 830-832 (2008).
- [33] J. D. Richmond-Decker, B.S. Thesis, Cornell University (2012).

## SUPPLEMENTARY INFORMATION

In this section, we give tables of three kinds of detailed information omitted from the main text of the paper.

### Al-Ir phases for stability calculations

Table III gives the data used to find the predicted binary phase diagram of the Al–Ir. system, by the usual convex-hull construction. Despite the structure names, a binary Al–Ir composition is used in all cases, with Ir replacing any transition metals. All energies are ab-initio calculations with the VASP code.

structure	$\Delta E$ meV/at.	$\Delta H$ meV/at.	x(Al) %	x(Ir) %
Al <sub>9</sub> Co <sub>2</sub> .mP22	0	-544.0	81.8	18.2
Al <sub>45</sub> Ir <sub>13</sub> .oP236	0	-658.8	77.6	22.4
Al <sub>21</sub> Pd <sub>8</sub> .tI116	0	-759.6	72.4	27.6
AlIr.cP2	0	-955.3	50.0	50.0
Al <sub>5</sub> Co <sub>2</sub> .hP28	2.8	-765.4	71.4	28.6
Al <sub>11</sub> Ir <sub>4</sub> .oP60 <sup>a</sup>	3.7	-737.9	73.3	26.7
Al <sub>41</sub> Ir <sub>23</sub> .hR64	5.6	-826.9	64.1	35.9
Al <sub>28</sub> Ir <sub>9</sub> .hP236	7.2	-672.3	76.5	23.5
Al <sub>3</sub> Ir.hP24 <sup>b</sup>	7.8	-722.5	73.9	26.1
Al <sub>11</sub> Ir <sub>4</sub> .oA236 <sup>c</sup>	9.2	-741.2	72.9	27.1
Al <sub>3</sub> Ir.hP8	25.0	-684.2	75.0	25.0

<sup>a</sup> “10-phase”

<sup>b</sup> triple supercell of Al<sub>3</sub>Ir, with one less Al atom (site vacant).

<sup>c</sup> “9.5-phase”

TABLE III: Energy diagram of Al–Ir system at T=0K. Column  $\Delta E$  is energy in meV/atom by which a structure is unstable relative to a mixture of competing stable compounds. Stable compounds forming convex hull of energy–composition scatter plot have  $\Delta E = 0$ .

	$C_1$	$\eta_1$	$C_2$	$\eta_2$	$k_*$	$\Phi_*$
Al-Al	$9.9811 \times 10^2$	8.7044	-11.3044	5.4518	3.5646	2.5119
Al-Ir	$1.3764 \times 10^4$	13.3271	9.2649	3.8320	3.1919	1.1091
Ir-Ir	$3.2083 \times 10^5$	12.7731	-7.2818	3.0765	-2.8274	0.4493

TABLE IV: Fitted parameters for Al-Ir EOPP potentials.

### Fitted pair potentials

Most calculations in the paper were based on empirical oscillating pair potentials” (EOPP) of form

$$V(r) = \frac{C_1}{r^{\eta_1}} + \frac{C_2}{r^{\eta_2}} \cos(k_* r + \phi_*) \quad (1)$$

as presented by Mihalkovič and Henley (main text Ref. [6]). where  $r$  is the distance between a pair of atoms. The fitted coefficients we used are listed in Table IV. Fig. 4 gives a scatter plot demonstrating the goodness of fit and a plot of the potentials themselves. As is typical of Al-transition metal (Al-TM) potentials, with TM=Ir in this case: (a) the Al-Al potential has no nearest-neighbor well but only a shoulder (b) the Al-Ir potential has a very deep well at the nearest-neighbor distance (c) the Ir-Ir potential is unfavorable for nearest neighbors but has a deep well at the second neighbor distance (d) all the potentials have relatively strong Friedel oscillations.

### Crystal structure of phase with $\text{Al}_{10}\text{Ir}$ clusters

Table V. lists all the Wyckoff positions of the low-temperature structure of the “10-phase” of  $\text{Al}_{11}\text{Ir}_4$ ; The cluster orientations correspond to Figure 1(b) of the main

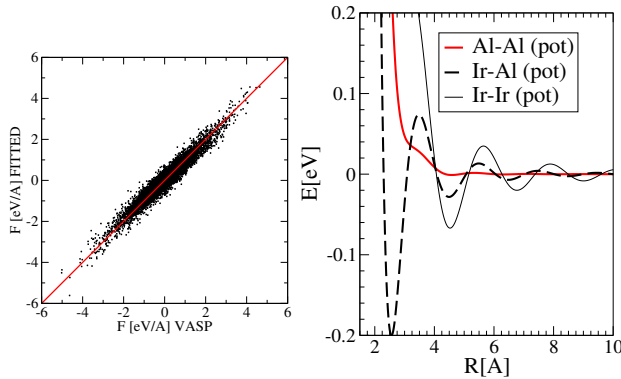


FIG. 4: EOPP potentials fitted to ab-initio (VASP) force and energy datapoints. Fit to forces (left panel) is shown with fitted forces (vertical axis) plotted against VASP forces (horizontal axis). The fitted pair potentials are shown in the right panel. Parameters

site	X	Y	Z	site	X	Y	Z
Ir1/2b	0.5000	0.5000	0.5135	Ir2/2c	0.2500	0.9952	0.0140
Ir3/2c	0.2500	0.4745	0.2897	Ir4/2c	0.2500	0.5099	0.7156
Ir5/4d	0.5028	0.7269	0.0113	Ir6/4d	0.3868	0.9996	0.5274
Al1/4d	0.5006	0.7884	0.6822	Al2/4d	0.3544	0.3333	0.5161
Al3/4d	0.3521	0.6752	0.5022	Al4/4d	0.5850	0.4755	0.2149
Al5/4d	0.5898	0.4900	0.8229	Al6/4d	0.5175	0.8086	0.3328
Al7/4d	0.3668	0.8794	0.2035	Al8/2c	0.2500	0.1771	0.7409
Al9/4d	0.4059	0.9910	0.8849	Al10/2c	0.7500	0.1536	0.7156
Al11/4d	0.6644	0.7314	0.0690	Al12/2c	0.2500	0.0944	0.3570
Al13/2c	0.2500	0.6492	0.0134				

TABLE V: List of Wyckoff sites for “10-phase” structure. Space group is  $Pma2$  (#28), Pearson symbol  $oP60$ . VASP-optimized lattice parameters are  $a=15.492\text{\AA}$ ,  $b=7.725\text{\AA}$  and  $c=7.685\text{\AA}$ .

site	X	Y	Z	site	X	Y	Z
Ir1/8d	0.7498	0.0006	0.0008	Ir2/4c	0.0003	0.2500	0.7498
Ir3/4c	0.7499	0.2500	0.6054	Ir4/8d	0.3602	0.0013	0.7517
Ir5/8d	0.5001	0.8857	0.4935	Ir6/4c	0.7506	0.7500	0.4015
Ir7/4c	0.5018	0.7500	0.2503	Ir8/4c	0.2619	0.2500	0.6151
Ir9/4c	0.2461	0.7500	0.3962	Ir10/8d	0.8581	0.9789	0.2506
Ir11/8d	0.0006	0.3900	0.4985	Al1/8d	0.3968	0.0026	0.9159
Al2/8d	0.1609	0.3489	0.5097	Al3/8d	0.2589	0.0888	0.1491
Al4/8d	0.2355	0.9163	0.1534	Al5/8d	0.1613	0.6470	0.4972
Al6/8d	0.2433	0.0876	0.8458	Al7/8d	0.3353	0.6469	0.5003
Al8/8d	0.3340	0.3545	0.5049	Al9/8d	0.2591	0.9076	0.8499
Al10/8d	0.4067	0.9853	0.0921	Al11/8d	0.9012	0.8370	0.3482
Al12/4c	0.5471	0.7500	0.5829	Al13/8d	0.4266	0.8563	0.6523
Al14/4c	0.4199	0.2500	0.3969	Al15/4c	0.5860	0.2500	0.3900
Al16/8d	0.4944	0.9075	0.8078	Al17/4c	0.3149	0.2500	0.2534
Al18/8d	0.9035	0.9986	0.9101	Al19/8d	0.9061	0.9990	0.0891
Al20/8d	0.3622	0.8352	0.2277	Al21/8d	0.0296	0.9100	0.2485
Al22/4c	0.0351	0.2500	0.5873	Al23/8d	0.8927	0.1643	0.6627
Al24/4c	0.1662	0.7500	0.2510	Al25/4c	0.0534	0.7500	0.4062

TABLE VI: Atomic structure of “9.5-phase” ( $oA236$ ) in space group  $Abm2$  (# 39). Optimized lattice parameters are  $a=15.321\text{\AA}$ ,  $b=15.475\text{\AA}$ ,  $c=15.412\text{\AA}$ . Cluster centers are Ir2 (“9-clusters”) and Ir7 (“10-clusters”).

text, corresponding to a cubic cell doubled in one direction (becoming the  $a$  direction); since the cubic structure lacks 4-fold symmetry, this causes the  $b$  and  $c$  cell parameters to become different by  $\sim 0.6\%$ .

site	X	Y	Z	site	X	Y	Z
Ir1/4b	0.5000	0.0000	0.2500	Ir2/8j	0.2497	0.2507	0.5000
Ir3/8j	0.9954	0.3955	0.5000	Ir4/16k	0.3926	0.2502	0.7704
Ir5/16k	0.2503	0.5011	0.3603	Ir6/8j	0.9997	0.1036	0.5000
Ir7/4a	0.0000	0.0000	0.7500	Al1/16k	0.8442	0.5900	0.2517
Al2/16k	0.0877	0.9954	0.3987	Al3/16k	0.4831	0.8460	0.1605
Al4/16k	0.9124	0.5012	0.1026	Al5/16k	0.9870	0.1541	0.3407
Al6/16k	0.1544	0.0893	0.7501	Al7/16k	0.1490	0.1544	0.4135
Al8/16k	0.1403	0.3379	0.4147	Al9/16k	0.2780	0.2536	0.6603
Al10/8j	0.2925	0.4107	0.5000	Al11/8j	0.3035	0.0941	0.5000
Al12/8j	0.4193	0.2521	0.5000				

TABLE VII: “9-phase” structure ( $oI232$ ), space group  $Ibam$  (# 72), orthorhombic lattice parameters are  $a=15.136$  Å,  $b=15.517$  Å,  $c=15.457$  Å. “9-cluster” centers are at Ir2 site.

site	X	Y	Z	site	X	Y	Z
Ir1/3a	0.0000	0.0000	0.0020	Ir2/3a	0.0000	0.0000	0.7488
Ir3/3a	0.0000	0.0000	0.2496	Ir4/9b	0.2685	0.2430	0.6356
Ir5/9b	0.6312	0.0770	0.4618	Ir6/9b	0.2696	0.9981	0.3618
Ir7/9b	0.3639	0.9178	0.5390	Ir8/3a	0.0000	0.0000	0.5959
Ir9/9b	0.7434	0.8712	0.4665	Ir10/3a	0.0000	0.0000	0.4027
Ir11/9b	0.2580	0.1292	0.5313	Al1/3a	0.0000	0.0000	0.4995
Al2/9b	0.8717	0.1251	0.4363	Al3/9b	0.1273	0.2493	0.5613
Al4/9b	0.2697	0.2245	0.2304	Al5/9b	0.0399	0.2553	0.2678
Al6/9b	0.0192	0.1585	0.1729	Al7/9b	0.1447	0.1397	0.3285
Al8/9b	0.7519	0.7866	0.7716	Al9/9b	0.9571	0.7422	0.7301
Al10/9b	0.9820	0.8361	0.8292	Al11/9b	0.8418	0.8617	0.6704
Al12/9b	0.5229	0.1744	0.4054	Al13/9b	0.1543	0.4314	0.6314
Al14/9b	0.8615	0.5862	0.3442	Al15/3a	0.0000	0.0000	0.9080

TABLE VIII: Structure of rhombohedral  $Al_{41}Ir_{23}$  ( $hR64$ ) phase, space group  $R3$  (# 146) in hexagonal setting. Optimized lattice parameters are  $a=11.032$  Å and  $c=27.073$  Å. “10-clusters” surround Ir1 sites, Al1 site is center of “B2”-structure local environments.